Neoplasia • Vol. 7, No. 11, November 2005, pp. 977–983

www.neoplasia.com

Novel Multiwavelength Microscopic Scanner for Mouse Imaging[1]

Herlen Alencar, Umar Mahmood*, Yoshihiro Kawano†, Tadashi Hirata† and Ralph Weissleder**

*Center for Molecular Imaging Research, Massachusetts General Hospital, Harvard Medical School, Charlestown, MA 02129, USA; †Bioscence Division, Bio-Business Development Department, Olympus Corporation, Tokyo 192-8512, Japan

Abstract

Real-time *in vivo* imaging of molecular targets at (sub)cellular resolution is essential in better understanding complex biology. Confocal microscopy and multiphoton microscopy have been used in the past to achieve this goal, but their true capabilities have often been limited by bulky optics and difficult experimental set-ups requiring exteriorized organs. We describe here the development and validation of a unique near-infrared laser scanning microscope system that uses novel optics with a millimeter footprint. Optimized for use in the far red and near-infrared ranges, the system allows an imaging depth that extends up to 500 μm from a 1.3-mm-diameter stick objective, which is up to 2 cm in length. We show exceptionally high spatial, temporal, and multiwavelength resolutions of the system and show that it can be applied to virtually any internal organ through a keyhole surgical access. We demonstrate that, when combined with novel far red imaging probes, it is possible to image the cellular details of many organs and disease processes. The new optics, coupled with the use of near-infrared probes, should prove immensely valuable for *in vivo* cancer imaging.

Neoplasia (2005) **7,** 977–983

Keywords: confocal microscopy, reconstruction, imaging, near-infrared, fluorescence.

Introduction

There has been a growing interest in adapting microscopic imaging approaches to study different disease processes and complex biology *in vivo*. One reason for this has been the growing realization that *in vivo* data can result in observations that are fundamentally different from those of *in vitro* experiments. A number of microscopic resolution imaging techniques have been developed to gain stunning insights into tumor pathophysiology [1–3] and the cellular tracking of immune cells [4,5] and stem cells [6]. Most tumor studies to date have relied on glass window preparations [1–3] or highly invasive procedures involving the exteriorization or complete exposure of entire organs [7–9]. Given the invasiveness of these procedures, a complete organ coverage and an improved depth penetration have been challenging. One approach to minimally invasive microscopy has been the introduction of miniaturized confocal microscopy systems. Several experimental devices based on fiber-optic approaches have been described [10–15], and some of them have been tested clinically [16]. Despite these advances, the fiber-optic approach places limitations on photon flux, thus limiting true video rate and multiwavelength imaging capabilities. This becomes even more accentuated with far red and near-infrared photons. This range travels through tissues most efficiently and is thus often used for whole animal imaging [17].

Given the above limitations, we set out to design a miniaturized laser scanning microscope for *in vivo* use. The system operates in the visible and near-infrared ranges at up to four wavelengths (three of which can be acquired simultaneously at any time). The optics of the system relies on 16-G-diameter (1.3-mm-diameter) "stick optics" that can be inserted into a subject through a tiny keyhole incision. Furthermore, the biopsy needle–sized objectives have a distal flush mechanism that allows their insertion deep (1–2 cm) into tumors or organs. We show that this approach allows for real-time imaging of most internal organs, including the colon, pancreas, bladder, liver, and brain. This system should be useful to simultaneously image different fluorescent proteins [18], transgenic reporter animals [19], and near-infrared reporter probes [17].

Materials and Methods

Miniaturized Laser Scanning Microscope

The microscope prototype and a schematic of the system design are shown in Figures 1 and 2. In the current setting, four lasers were used for excitation: 1) a 488-nm air-cooled argon laser, with 40 mW of power output (Model IMA101040ALS; Melles Griot, Carlsbad, CA); 2) a 561-nm solid-state yellow laser, with 1 mW of power output (Model 85YCA010; Melles Griot); 3) a 633-nm HeNe–R laser, with 10 mW of power output (Model 05LHP925; Melles Griot); and 4) a 748-nm infrared diode laser, with 30 mW of power output (Model FV10-LD748;

Address all correspondence to: Ralph Weissleder, Center for Molecular Imaging Research, Massachusetts General Hospital, Harvard Medical School, Building 149, 13th Street, No. 5408, Charlestown, MA 02129. E-mail: weissleder@helix.mgh.harvard.edu

[1]The study was supported, in part, by R24CA92782, P50CA86355, and a grant from the New Energy and Industrial Technology Development Organization.

Received 1 June 2005; Revised 1 June 2005; Accepted 14 July 2005.

DOI 10.1593/neo.05376

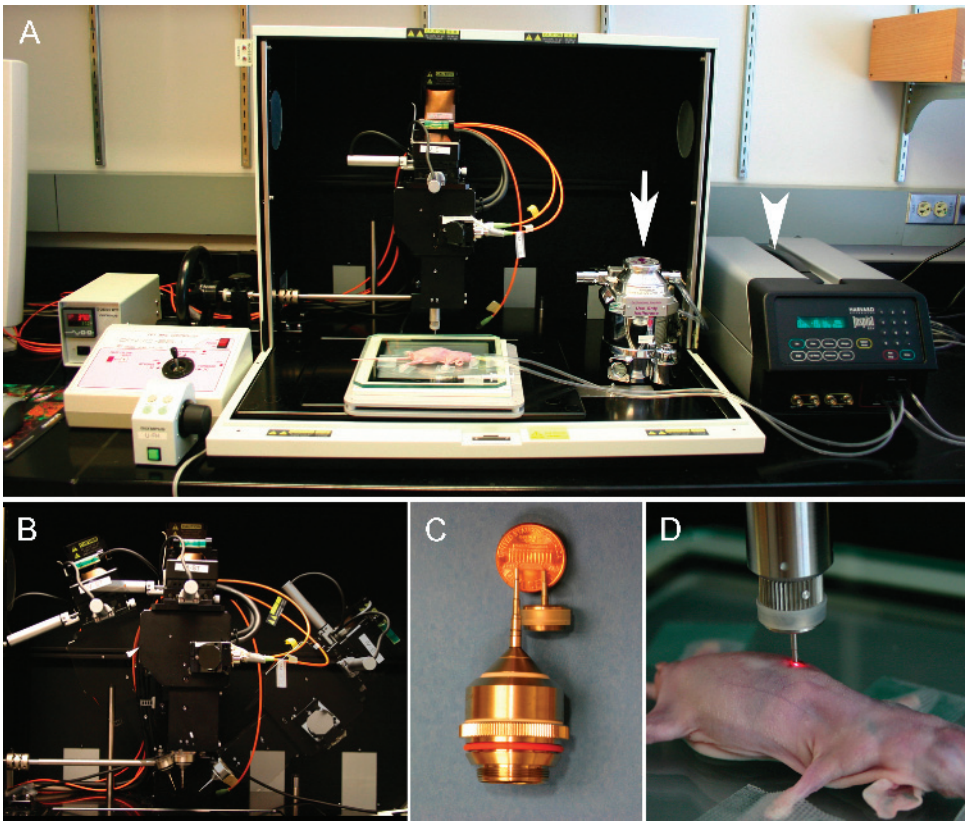

Figure 1. *Prototype of the laser scanner developed. (A) The system has an integrated gas vaporizer (arrow) and ventilator (arrow head), allowing for surgical procedures to be performed on the imaging stage. (B) The microscope head containing the acquisition chamber can be tilted from -10° to 70° to either side, minimizing animal repositioning and facilitating the imaging of uneven or curved organ surfaces. (C and D) New stick objectives allow a minimally invasive microscopy of internal organs through keyhole incisions.*

Olympus Corporation, Tokyo, Japan). The conventional plan apochromat and plan semiapochromat objectives were designed for optimal performance with fluorescent microscopy (Table 1). The novel stick objectives (the smallest objectives developed to date for laser scanning microscopy) were designed specifically for this laser scanning microscope. They deliver high-resolution images in the visible light and near-infrared spectrum and can be used to image virtually any internal organ through small incisions due to their reduced footprint size (1.3 mm in external diameter).

Wide spectral response photomultiplier tubes (model R928P; Hamamatsu Photonics, Hamamatsu City, Japan) were used as detectors to provide a high quantum efficiency and amplification for both visible light and near-infrared signals.

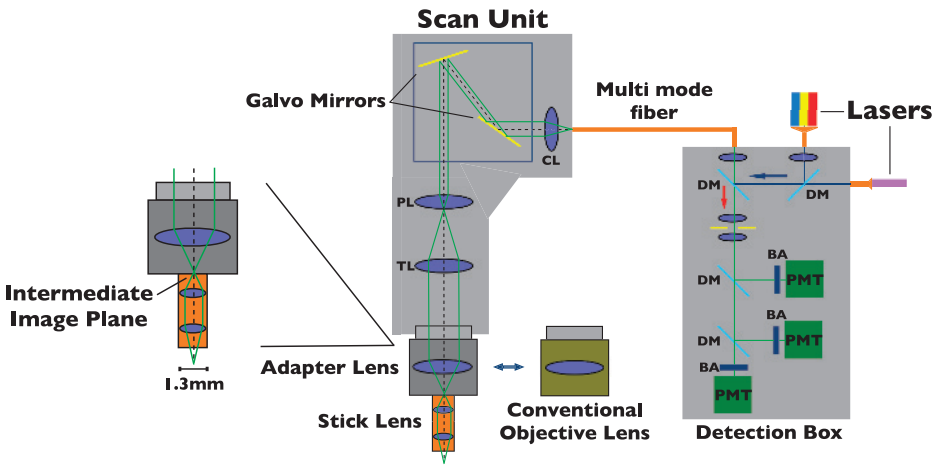

Figure 2. *A schematic showing the system design (please see the text for details). BA, band-pass filter; PMT, photomultiplier tube; DM, dichroic mirror; CL, collector lens; PL, pupil lens; TL, tube lens.*

Table 1. Objectives.

Magnification	Field of View	Working Distance	Immersion	Description
×4	3.25 mm	13 mm	No	UPLFL
×10	1.3 mm	10 mm	No	UPLFL
×10	1.3 mm	3.1 mm	No	UPLAPO
×20	0.65 mm	1.6 mm	No	UPLFL
×40	0.325 mm	0.51 mm	Water	UPLFL
×20 SS	200 μm	100 μm	Water	MLS-D1W100W
×30 SS A	260 μm	50 μm	Water	MLS-D3W050W
×30 SS B	260 μm	200 μm	Water	MLS-D3W200W
×6 LS	670 μm	200 μm	No	IV-OB13F67W20
×20 LS	200 μm	200 μm	Water	IV-OB13F20W20
×27.3 LS	220 μm	200 μm	Water	IV-OB35F22W20

All stick objectives were custom-developed for the current study. SS, short stick objective; LS, long stick objective.

Olympus Corporation custom-built dichroic mirrors (SDM-570, SDM-630, SDM-633, and SDM-750), long-pass filter (BA 770 nm IF) and band-pass filters (BA 505–525 nm, BA 585–615 nm, and BA 660–730 nm) were applied in an appropriate sequence to detect up to three wavelengths simultaneously.

To further expand the ability of the microscope to image living mice and to allow for surgical procedures to be performed on the microscope stage, an isoflurane vaporizer (Braintree Scientific, Braintree, MA) and a small animal volume-controlled ventilator (Inspira ASV; Harvard Apparatus, Holliston, MA) were built into the system. A PC computer running FluoView software (Olympus Corporation) was used to control the microscope, and all images were recorded and stored as proprietary multilayer 16-bit Tagged Image File Format files.

Probes

A near-infrared imaging probe was used to image the microvasculature of different organs and diseases processes (Angiosense-750; Visen Medical, Woburn, MA). This probe circulated inside normal blood vessels for up to 2 hours. Excitation was provided by the 748-nm infrared laser, and emission was capture in the AF750 channel (770 nm long-pass filter).

A protease-activatable imaging probe was used to reveal cathepsin B activity in intestinal adenomas (Prosense-680; Visen Medical). Excitation was provided by the HeNe–R laser (633 nm) and emission capture in the Cy5.5 channel (660–730 nm band-pass filter). SYTOX green (Molecular Probes, Eugene, OR), a nucleic acid staining agent, was used to visualize the normal intestinal mucosa. This small molecule quickly extravasates from intestinal microvessels after intravenous injection and provides an anatomic background image that helps in the identification of adenomas. Excitation for SYTOX green was provided by the argon laser (488 nm), and the emission was captured in the green fluorescent protein (GFP) channel (505–525 nm band-pass filter).

For cell tracking experiments, animals were injected intravenously with rhodamine 6G (Molecular Probes). This probe specifically stains mitochondria of white blood cells, providing a strong fluorescent signal that allows the imaging of individual cells in the bloodstream. Excitation was provided by the 561-nm solid-state yellow laser, and emission was captured in the rhodamine channel (585–615 nm band-pass filter).

Animal Models

All animal studies were approved by the Institutional Animal Care Committee. For microvasculature imaging experiments, two transgenic mouse models are used. The GFP mouse [FVB.Cg–Tg(GFPU)5Nagy/J; Jackson Laboratory, Bar Harbor, ME] expresses GFP ubiquitously, and all organs and tissues are brightly fluorescent on 488-nm laser excitation. The Tie2 mouse [STOCK Tg(TIE2GFP)287Sato/J; Jackson Laboratory] expresses GFP under the control of the endothelial-specific receptor tyrosine kinase (Tek; formerly Tie2) promoter. In this case, only endothelial cells are green fluorescent. Mice were anesthetized (2% isoflurane in 2 l/min O_2), intubated, and connected to the small animal volume-controlled ventilator. Pancuronium (0.4 mg/kg) was administered intravenously to paralyze all skeletal muscles to reduce motion artifacts. Following animal anesthesia and positioning, Angiosense-750 (10 nmol/mouse) was injected intravenously prior to imaging, and small abdominal incisions were performed to expose the organ of interest. To image the bone marrow, mice were positioned in a stereotactic head frame, a small longitudinal skin incision was performed to exposed the skull, and images were acquire through intact bone.

The APCMin+/– mouse was used as a model for intestinal adenomatosis and protease overexpression, This well-established model mimics the rapid development of adenomatous polyps in humans with familial adenomatous polyposis. APCMin+/– mice develop spontaneous adenomas throughout the intestinal tract with aging. Animals were anesthetized, intubated, and paralyzed as described above. Prosense-680 (2 nmol/mouse) was injected 24 hours prior to imaging. SYTOX green and Angiosense-750 (10 nmol/mouse) were injected 30 minutes before imaging. Animals were positioned under the microscope, a small abdominal incision was made, and a loop of jejunum was identified for imaging. Microscopy was carried out using a simultaneous triple excitation (488, 633, and 748 nm), and image series was recorded in a similar fashion.

For cell tracking experiments, the ear of a nude mouse (nu/nu; Charles River Laboratories, Wilmington, MA) was injected subcutaneously with 5 ng/50 μl of recombinant mouse TNF-alfa (R&D Systems, Minneapolis, MN). Twenty-four hours later, rhodamine 6G (0.3 mg/kg) and Angiosense-750 were injected intravenously. The animal was then anesthetized (2% isoflurane in 2 l/min O_2), and images were acquired using double excitation (561 and 743 nm).

In the solid tumor imaging experiment, a colon cancer cell line transfected to stably express the fluorescent protein DsRed was used. Cells (1×10^6) were orthotopically implanted in the colon of a nude mouse and allowed to grow for 14 days. Immediately before imaging, Angiosense-750 was injected intravenously. The animal was anesthetized (2% isoflurane in 2 l/min O_2), and a small abdominal incision was performed to expose the colonic tumor. Images were acquired using double excitation (561 and 743 nm).

Results

System Performance

The near-infrared laser scanning imaging system design described here was optimized for small animal imaging using a multiwavelength approach with both visible light and near-infrared optical probes. The tiltable microscope head can be adjusted for the imaging of uneven and rounded surface organs with optimal excitation and minimal animal repositioning. The use of the newly designed stick objectives with millimeter footprint allowed the microscopic visualization of internal organs in a mouse through keyhole incisions. The combination of high-magnification stick objectives, minimal organ exposure, and the anesthesia and mechanical ventilation capabilities built into the system permits a serial imaging of virtually any deep abdominal organ. The small incisions needed to expose and image an anatomic region also reduce manipulation artifacts, especially trauma to the microvasculature.

The developed stick lenses have a resolution comparable to regular objectives and can resolve single cells and subcellular details, even when used in a multiwavelength approach. Importantly, photon flux measured at the tip of the stick objectives was sufficient to provide an appropriate excitation for all channels under normal imaging conditions (Figure 3). The system was capable of exciting up to four different fluorochromes at the same time and of acquiring up to three fluorescent channels simultaneously in real time. At the maximum scanning speed and using a matrix size of 256 $\times$ 256 pixels, the microscope generates video images at a rate of 2.2 frames/sec. The fluorochrome detection limit for all channels is in the femtomole range. The focal depth of the system is $\sim$500 μm, comparable to current multiphoton systems.

Imaging Microvascularity of Internal Organs

The combination of GFP-expressing transgenic mice, multiwavelength imaging, and intravascular near-infrared probes allowed the imaging of microvessels in normal internal organs as well as in more superficial vessels. Figure 4*A* shows a characteristic tortuous blood vessel in a GFP mouse bladder. The green background reveals the typical random distribution of detrusor muscle fibers. Figure 4*B* shows a straight blood vessel and its branches in a GFP mouse thigh. In the background, the parallel distribution typical of skeletal muscle fibers can be appreciated. In both cases, blood flowing through small capillaries embedded in the muscle fibers can be seem during real-time image acquisition, with individual blood cells seen as dark foci within the microvasculature.

When we used Tie2 mice, the green endothelial cells provided information about blood vessel location and distribution in the organs of interest. Figure 4*C* shows larger blood vessels and various smaller branches in the intact jejunal wall of a Tie2 mouse. When the intravascular probe is injected, the blood flow pattern and timing can be determined. Figure 4*D* shows the kidney of a Tie2 mouse imaged using a $\times$20 stick objective and a small flank incision. The nuclei of individual cells in kidney glomeruli are easily identified. The intravascular probe delineates blood vessel lumen and reports on blood flow pattern and distribution. Using the same objective and a small abdominal incision, we imaged the liver (Figure 4*E*) of a Tie2 mouse. Although bile autofluorescence signal generates noise in the GFP channel, green endothelial cells can be identified and the intravascular probe can be detected inside the blood vessels.

To test the system's ability to image blood flow in the bone marrow through intact bones, a small skin incision was made and the skull of a C57BL6/J mouse was exposed. Images

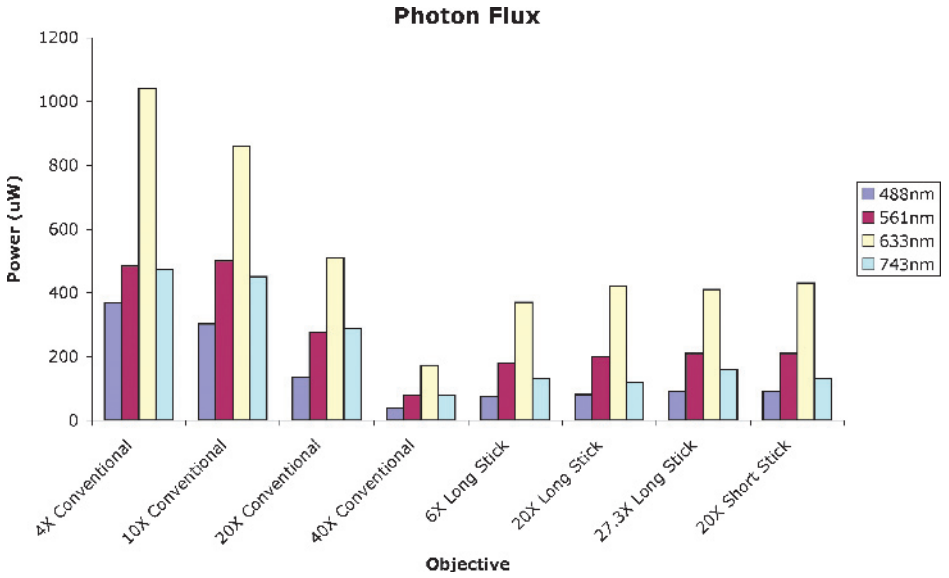

Figure 3. *A graph showing photon flux through the different objectives. The y-axis shows the photon flux measured at the tip of each objective. Despite their reduced footprint, stick objectives deliver adequate excitation light to the samples and provide high-resolution images from visible light to the near-infrared region.*

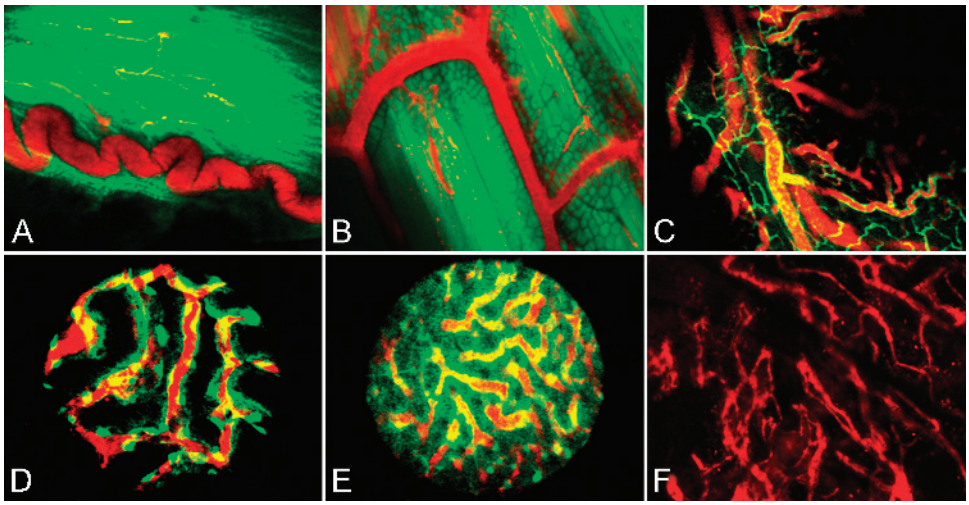

Figure 4. *Imaging of different organs in mouse models. (A) GFP mouse bladder wall imaged using a ×10 regular objective. A typical curled blood vessel (red) embedded into the detrusor muscle fibers (green). (B) A GFP mouse thigh imaged using a ×20 regular objective. Submillimeter vessels (red) are easily identified among skeletal muscle fibers. (C) A Tie2 mouse intact jejunal wall imaged using a ×20 regular objective. Endothelial cells (green) show microcirculation architecture, whereas the intravascular probe (red) reports on blood flow distribution. (D) A Tie2 mouse kidney imaged using a ×20 stick objective through a small flank incision. Individual endothelial cells (green) form the typical glomerular structure of the organ. The intravascular probe (red) is used to show blood flowing through the kidney. (E) A Tie2 mouse liver imaged using a ×20 stick objective. The image is acquired through a small abdominal incision, avoiding manipulation artifacts. (F) A C57BL6/J mouse skull bone marrow imaged using a ×10 regular objective. The intravascular probe (red) can be imaged through intact bones in this region.*

acquired after an Angiosense-750 injection showed the marrow trabecular structure in sharp detail (Figure 4*F*). We acquired thin-slice Z-stack images up to a maximum penetration of 500 μm. When time series were recorded, the negative contrast formed by individual blood cells flowing through bone marrow channels demonstrated flow.

We next used an ear inflammation model (Figure 5*A–I*) to track cellular homing to microvessels. Simultaneous images in the rhodamine channel clearly resolved individual white blood cells labeled with rhodamine 6G and their interactions with the endothelial surface of those microvessels. Time series images showed different rolling velocities of these white blood cells.

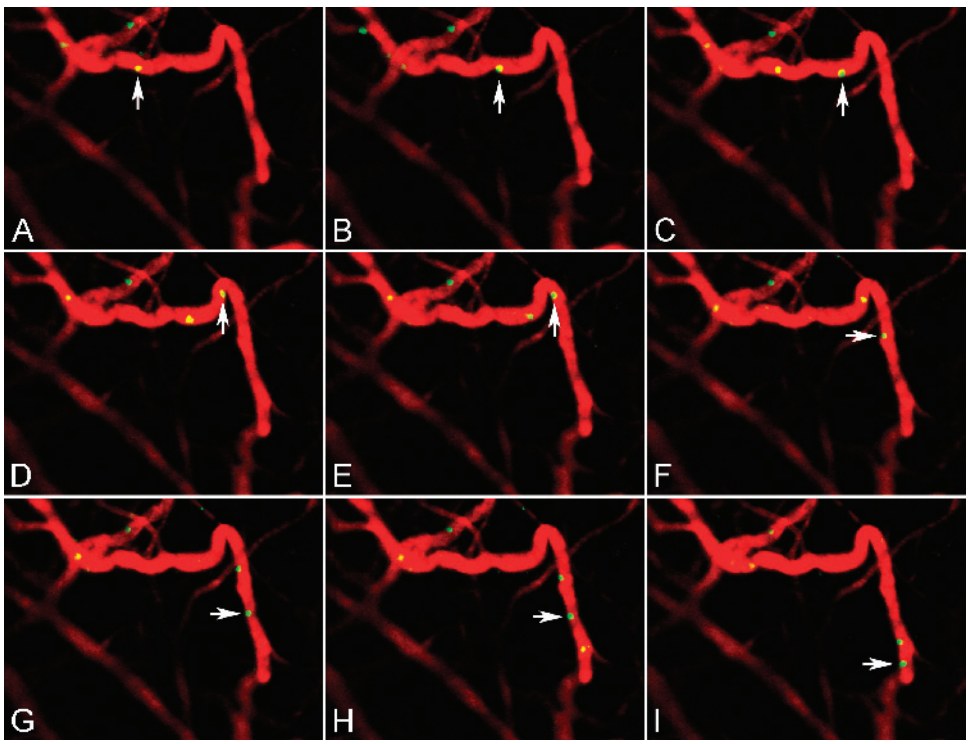

Figure 5. *Cell tracking in a mouse ear inflammation model. (A–I) Still frames from a 60-second movie showing single cells labeled with rhodamine 6G rolling (yellow) in the endothelial surface of a microvessel after intravascular probe (red) injection.*

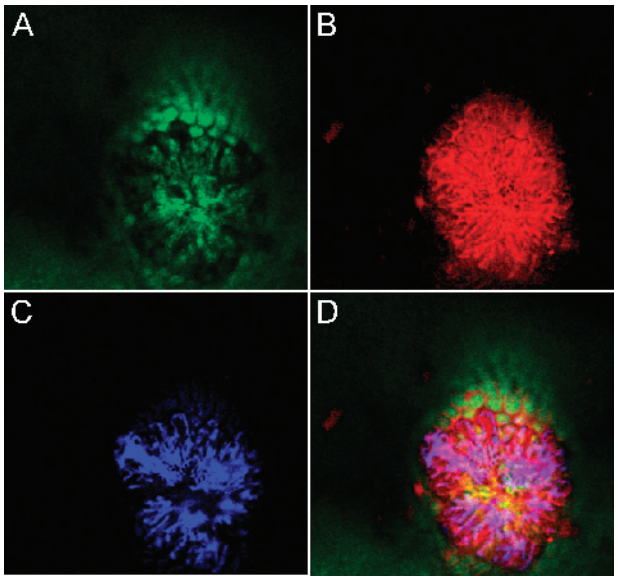

Figure 6. *Multichannel images of an intestinal adenoma in a APCMin+/− mouse. (A) The GFP channel shows a SYTOX green unspecific staining of the intestinal mucosa. (B) The Cy5.5 channel detecting protease overexpression in the adenoma when compared to the normal mucosa. (C) The AF750 channel showing abnormal blood vessels supplying the adenoma. (D) A merged image highlights the microscope's ability to combine structural and functional information to "dissect" submillimeter-sized structures.*

Imaging Host Interaction in Oncogenesis

Intestinal adenomas in aged APCMin+/− mice were imaged using three different probes and a simultaneous triple excitation. Figure 6*A* (GFP channel) shows the intestinal mucosa after a SYTOX green intravenous injection. This anatomic background helps in the differentiation between the normal mucosa and the epithelium overlying the adenomatous lesion. Figure 6*B* (Cy5.5 channel) shows the signal generated by an activation of the protease probe. Protease overexpression in intestinal adenomas is responsible for the stronger signal over the lesion. Figure 6*C* (AF750 channel) shows irregular, leakier blood vessels supplying the adenoma after an Angiosense-750 intravenous injection. The blood vessel density in the adenoma is clearly higher than in the normal adjacent mucosa. The merged image (Figure 6*D*) highlights the ability of this system to dissect a microscopic structure in a living animal using novel optical probes and a multiwavelength approach.

When a nude mouse bearing DsRed-positive orthotopic colon cancer was imaged, the blood supply to the tumor was clearly highlighted due to the intravascular probe injected prior to imaging (Figure 7*A*). Expression of the fluorescent protein DsRed by tumor cells was also identified in this multichannel setting (Figure 7*B*), demonstrating the ability of the system to characterize vascular supply to the tumor in its orthotopic colon bed.

Discussion

We set out to design a new laser scanning microscopy imaging system, which is specifically optimized for *in vivo* imaging of mouse models. A number of design criteria were first established. The system had to: 1) have the capability to resolve far red and near-infrared fluorescence because light penetrates most efficiently at these wavelengths and because there is low autofluorescence; 2) provide at least three to four channel multiwavelength capabilities without spectral overlap; 3) obviate the need for bulky optics with short working distances; 4) be compatible with anesthesia and ventilation support; 5) be able to achieve at least a 400-μm depth penetration from the tip of the lens; and 6) result in image qualities similar to those accustomed with commercial confocal and multiphoton systems.

We decided to completely incorporate digital image acquisition, relying on a novel design for a tiltable scan head (−10° to 70°) controllable electronically, similarly as in automated surgery. The newly designed stick objectives with millimeter footprint allowed the positioning of the lens through small incisions and the image acquisition of virtually any internal organ. The stick lenses had a resolution comparable to regular objectives and were able to resolve single cells and subcellular details, even when used in a multiwavelength approach.

We applied the system to imaging a number of different organs, physiological processes, and disease states to demonstrate its *in vivo* utility. As is evident from the images obtained (Figures 4–7), image quality was superb. Internal

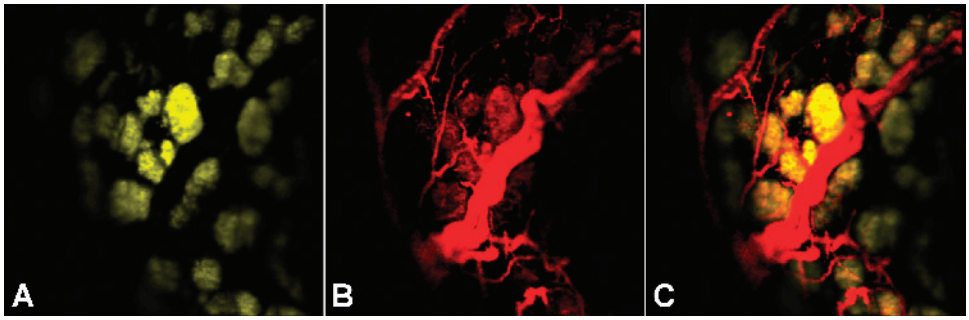

Figure 7. *Orthotopically implanted DsRed-positive colon tumor in a nude mouse imaged using double excitation. (A) The rhodamine channel showing the DsRed-expressing colon cancer cells 14 days after implantation. (B) The AF750 channel showing microvessels supplying the tumor. (C) Merged image.*

GFP and DsRed production in tumors, in microvessels, and during viral transfer could be readily detected. Using near-infrared markers of microvascular integrity and/or proteolysis, we were also able to characterize different disease processes such as tumoral angiogenesis, invasion, microvascular leak during rheumatoid arthritis formation, and reperfusion injury in intestinal ischemia, among others. The newly developed system should be widely useful to expand the capabilities of current microscopic imaging systems to *in vivo* imaging in experimental mouse models.

Acknowledegements

The authors would like to thank Mikael Pittet for discussions on cellular imaging and Alexei Bogdanov for providing the colon cancer cell line.

References

[1] Alexandrakis G, Brown EB, Tong RT, McKee TD, Campbell RB, Boucher Y, Jain RK (2004). Two-photon fluorescence correlation microscopy reveals the two-phase nature of transport in tumors. *Nat Med* **10** (2), 203–207.

[2] Brown E, McKee T, diTomaso E, Pluen A, Seed B, Boucher Y, Jain RK (2003). Dynamic imaging of collagen and its modulation in tumors *in vivo* using second-harmonic generation. *Nat Med* **9** (6), 796–800.

[3] Brown EB, Campbell RB, Tsuzuki Y, Xu L, Carmeliet P, Fukumura D, Jain RK (2001). *In vivo* measurement of gene expression, angiogenesis and physiological function in tumors using multiphoton laser scanning microscopy. *Nat Med* **7** (7), 864–868.

[4] Mempel TR, Henrickson SE, and Von Andrian UH (2004). T-cell priming by dendritic cells in lymph nodes occurs in three distinct phases. *Nature* **427** (6970), 154–159.

[5] von Andrian UH (2002). Immunology. T cell activation in six dimensions. *Science* **296** (5574), 1815–1817.

[6] Sipkins DA, Wei X, Wu JW, Runnels JM, Cote D, Means TK, Luster AD, Scadden DT, Lin CP (2005). *In vivo* imaging of specialized bone marrow endothelial microdomains for tumor engraftment. *Nature* June **16**; 435(7044):969–973.

[7] Ito S, Nakanishi H, Ikehara Y, Kato T, Kasai Y, Ito K, Akiyama S, Nakao A, Tatematsu M (2001). Real-time observation of micrometastasis formation in the living mouse liver using a green fluorescent protein gene–tagged rat tongue carcinoma cell line. *Int J Cancer* **93** (2), 212–217.

[8] Keck T, Campo-Ruiz V, Warshaw AL, Anderson RR, Fernandez-del Castillo C, Gonzalez S (2001). Evaluation of morphology and microcirculation of the pancreas by *ex vivo* and *in vivo* reflectance confocal microscopy. *Pancreatology* **1** (1), 48–57.

[9] Mook OR, Van Marle J, Vreeling-Sindelarova H, Jonges R, Frederiks WM, Van Noorden CJ (2003). Visualization of early events in tumor formation of eGFP-transfected rat colon cancer cells in liver. *Hepatology* **38** (2), 295–304.

[10] Bonnans V, Gharbi T, Pieralli C, Wacogne B, Humbert P (2004). New fluorescence imaging probe with high spatial resolution for *in vivo* applications. *J Biomed Opt* **9** (5), 928–933.

[11] Carlson K, Chidley M, Sung KB, Descour M, Gillenwater A, Follen M, Richards-Kortum R (2005). *In vivo* fiber-optic confocal reflectance microscope with an injection-molded plastic miniature objective lens. *Appl Opt* **44** (10), 1792–1797.

[12] Gobel W, Kerr JN, Nimmerjahn A, Helmchen F (2004). Miniaturized two-photon microscope based on a flexible coherent fiber bundle and a gradient-index lens objective. *Opt Lett* **29** (21), 2521–2523.

[13] Laemmel E, Genet M, Le Goualher G, Perchant A, Le Gargasson JF, Vicaut E (2004). Fibered confocal fluorescence microscopy (Cell-viZio) facilitates extended imaging in the field of microcirculation. A comparison with intravital microscopy. *J Vasc Res* **41** (5), 400–411.

[14] McLaren WJ, Anikijenko P, Thomas SG, Delaney PM, King RG (2002). *In vivo* detection of morphological and microvascular changes of the colon in association with colitis using fiberoptic confocal imaging (FOCI). *Dig Dis Sci* **47** (11), 2424–2433.

[15] Rouse AR, Kano A, Udovich JA, Kroto SM, Gmitro AF (2004). Design and demonstration of a miniature catheter for a confocal microendoscope. *Appl Opt* **43** (31), 5763–5771.

[16] Kiesslich R, Burg J, Vieth M, Gnaendiger J, Enders M, Delaney P, Polglase A, McLaren W, Janell D, Thomas S, et al. (2004). Confocal laser endoscopy for diagnosing intraepithelial neoplasias and colorectal cancer *in vivo*. *Gastroenterology* **127** (3), 706–713.

[17] Weissleder R and Ntziachristos V (2003). Shedding light onto live molecular targets. *Nat Med* **9** (1), 123–128.

[18] Shaner NC, Campbell RE, Steinbach PA, Giepmans BN, Palmer AE, Tsien RY (2004). Improved monomeric red, orange and yellow fluorescent proteins derived from *Discosoma* sp. red fluorescent protein. *Nat Biotechnol* **22** (12), 1567–1572.

[19] Hoffman RM (2004). Imaging tumor angiogenesis with fluorescent proteins. *APMIS* **112** (7–8), 441–449.